Journal of Materials Chemistry A

Accepted Manuscript

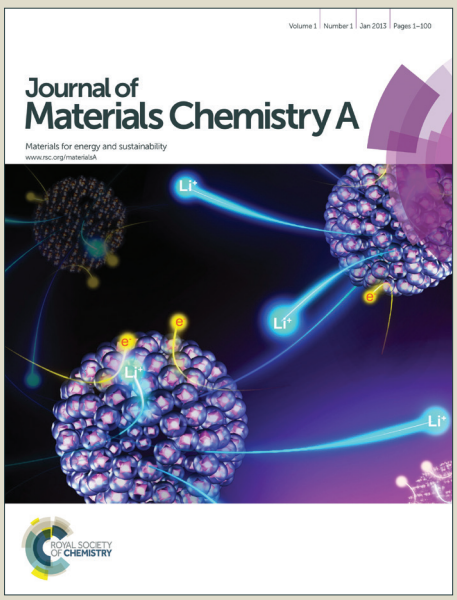

ROYAL SOCIETY OF CHEMISTRY

www.rsc.org/materialsA

A Table of Contents Entry

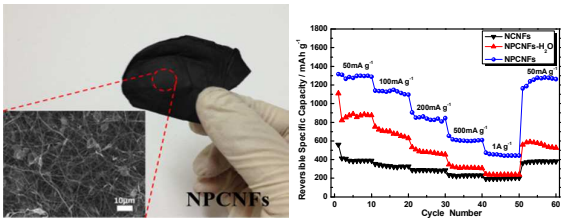

Nitrogen-enriched electrospun carbon nanofiber networks were prepared for a free-standing LIB anode material with ultrahigh capacity and good rate capability.

Journal of Materials Chemistry A

RSCPublishing

ARTICLE

Nitrogen-enriched Electrospun Porous Carbon Nanofiber Networks as High-performance Free-standing Electrode Materials

Cite this: DOI: 10.1039/x0xx00000x

Received 00th January 2012,
Accepted 00th January 2012

DOI: 10.1039/x0xx00000x

www.rsc.org/

Ding Nan[ad], Zheng-Hong Huang[b*], Ruitao Lv[b], Lu Yang[b], Jian-Gan Wang[b], Wanci Shen[b], Yuxiao Lin[b], Xiaoliang Yu[b], Ling Ye[b], Hongyu Sun[b], Feiyu Kang[bc*]

Nitrogen-enriched porous carbon nanofiber networks (NPCNFs) were successfully prepared by using low-cost melamine and polyacrylonitrile as precursors via electrospinning followed by carbonization and NH_3 treatments. The NPCNFs exhibited interconnected nanofibrous morphology with large specific surface area, well-developed microporous structure, relatively high-level nitrogen doping and great amount of pyridinic nitrogen. As free-standing new anode materials in lithium-ion batteries (LIBs), NPCNFs showed ultrahigh capacity, good cycle performance and superior rate capability with a reversible capacity of as high as 1323 mAh g^{-1} at a current density of 50 mA g^{-1}. These attractive characteristics make the NPCNFs materials as very promising anode candidates for high-performance LIBs and, as free-standing electrode materials to be used in other energy conversion and storage devices.

1. Introduction

Lithium ion batteries (LIBs) have attracted great attention from both scientific community and industry due to their significant advantages over traditional rechargeable battery systems (*e.g.* lead-acid batteries, nickel-cadmium batteries, nickel-metal hydride batteries *et al.*). So far, LIBs have been widely used in powering diverse mobile electronic devices. Recently, larger scale applications of LIBs, including various types of electrical vehicles (EVs) and energy storage for utility grids, are also rapidly developing[1-5]. Nowadays, the most commonly used anode material for commercial LIBs is graphite. However, graphite cannot meet the increasing demands for LIBs in different fields due to their low theoretical specific capacity (372 mAh g^{-1}) and poor rate capability [6]. In this context, much efforts have been paid to explore new anode materials with enhanced Li-ion storage capacity, *i.e.* carbonaceous materials[7-23], alloys[24], metal oxides[25, 26] and their hybrids[27, 28]. Among them, porous carbon nanostructures can facilitate easy access of Li-ion transport and promote charge-transfer reaction by offering more electrode/electrolyte interface, and thus are very promising for developing high-performance anode materials.

Moreover, chemical doping of carbon materials with heteroatoms, such as phosphorus[29, 30], sulfur[31], boron[32-34], nitrogen[14-16, 35-47] and boron-nitrogen[48], is an efficient way to tailor their electronic and chemical properties. Among different dopants, nitrogen has attracted the most attention due to the following reasons. Firstly, nitrogen has a comparable atom size with carbon and its electronegativity (3.04) is higher than that of carbon (2.55). Thus the nitrogen is easier to bond with carbon atoms and more favorable for lithium insertion[15]. Moreover, nitrogen doping can create defect sites for lithium storage[49]. Hence it can substantially increase the Li-ion storage capacity. Secondly, N doping in carbon materials can greatly enhance the electronic conductivity and induce *n*-type conducting behaviors, because N can introduce donor states near the Fermi level. Therefore, for the carbon-based anode materials, porous nanostructure with nitrogen incorporation are highly desirable for achieving excellent LIB performance, such as high lithiation capacity, good rate capability and long-term cycling stability. Based on this concept, a few previous reports have shown that nitrogen-doped porous carbon materials can serve as excellent anode materials for LIBs. For instance, Mao *et al.*[15] prepared a kind of nitrogen-rich mesoporous carbon materials by pyrolyzing gelatin using a sacrificial nano-$CaCO_3$ template with very good electrochemical performances. It showed a high reversible capacity of 1024 mAh g^{-1} in first cycle and stabilized to *ca.* 900 mAh g^{-1} after 40 cycles at a current density of 0.1 mA cm^{-1}. Qie *et al.*[16] used a modified oxidative template assembly route to synthesize a kind of nitrogen-doped porous carbon nanofiber networks. Compared with granular carbons, it exhibited better electrochemical performance, with the first cycle reversible capacity reaching as high as 1280 mAh g^{-1} at a current density of 0.1 A g^{-1}.

In addition, in conventional protocol for preparing LIB electrodes, binder materials, such as polyvinylidene fluoride (PVDF), are usually required for improving the mechanical stability of electrodes, but binders will unavoidably reduce the electrical conductivity and block the pores. Moreover, binders will limit the applications of LIBs in high-temperature areas (*e.g.* above 200 °C) due to their instability. In this sense, developing binder-free electrodes will be a promising technique to simplify electrode preparation process, reduce the cost, and

develop future high-performance LIBs. The key issue for binder-free electrodes is to synthesize robust free-standing electrode materials. Recently, some exciting progress has been made along this direction[8, 17, 18, 20]. However, the capacity (*e.g.* 450 mAh g^{-1} [8], 593 mAh g^{-1} [17], 566 mAh g^{-1} [18], 730 mAh g^{-1} [20]) and cycling stability of LIB with as-synthesized free-standing electrode materials still needs to be improved. In addition, developing low-cost synthesis technique for free-standing electrode materials will be favorable for their future commercial applications.

In virtue of the simple procedure, low cost and scale-up potential, electrospinning has been extensively investigated for preparing porous carbon nanofiber fabrics (PCNFs) recently [17, 18, 20, 50]. As-prepared PCNFs fabrics are typically arranged in an interconnected non-woven networks, which can provide good mechanical integrity at the same time. Such fabrics can be used as free-standing anodes for LIBs, and it would increase the effective electrode-electrolyte interface area, ensuring high energy and power delivery, long cycling stability and improved safety of LIBs. However, there is almost no report on using electrospinning to synthesize free-standing nitrogen-doped porous carbon materials with excellent electrochemical performance so far.

In this communication, we report a simple, scalable and inexpensive approach for the preparation of nitrogen-enriched porous carbon nanofiber networks (NPCNFs) using electrospinning along with the subsequent carbonization and NH_3 treatments. As-synthesized NPCNFs demonstrate a large surface area and a relatively high nitrogen doping level. They can be used as an excellent free-standing LIB anode material, with ultrahigh capacity and good rate capability. Furthermore, as-synthesized NPCNF networks may find wide applications in diverse areas, such as sodium-ion batteries, supercapacitors, lithium–sulfur batteries, lithium–air batteries and other energy conversion/storage devices.

2. Experimental

2.1. Materials synthesis

Firstly, Polyacrylonitrile (PAN) (Mw = 150,000, homopolymer, SP[2] company, USA) was dissolved in N,N-dimethylfomamide (DMF) with concentration of 10 wt% to form a homogenous solution, and a certain amount of melamine was add into the PAN/DMF solution (the mass ratio of melamine and PAN was 1:2), then both of the solutions were vigorously stirred in water bath at 70 °C for 12 h to obtain the precursors of electrospinning for raw nanofibers (PAN) and nitrogen doped raw nanofibers (NPAN). Then the as-prepared precursors were electrospun into fiber networks through a positively charged capillary using an electropspinning apparatus at 25 kV. A piece of graphite paper was used as the collector. The distance of tip and the collector was 15 cm, and the flow rate of the spinning solution was 1 ml h^{-1}.

The electrospun-derived fiber networks were stabilized under air according to a temperature program, in which it was heated at a rate of 5 °C min^{-1} up to 250 °C and held for 1h, and then the temperature was raised to 260 °C and 270 °C at a rate of 2 °C min^{-1} and held for 1h and 2h, respectively. The stabilized nanofiber networks were heated at a rate of 5 °C min^{-1} for up to 850 °C in nitrogen for 1h to obtain carbon nanofiber networks (CNFs) and nitrogen-doped carbon nanofiber networks (NCNFs). Then for activation, the NCNFs were treated by 20 vol% of ammonia in nitrogen for 30 mins to obtain nitrogen-enriched porous carbon nanofiber networks (NPCNFs). For comparison purpose, nitrogen-enriched porous carbon nanofiber networks activated by 20 vol% water steam in nitrogen for 30 mins were prepared and denoted as NPCNFs-H_2O.

2.2. Characterization

The morphology and microstructure of samples was characterized with a scanning electron microscope (SEM, LEO 1530, Germany) and transmission electron microscopy (TEM, JEOL 2010, Japan). The TEM specimens were prepared by dispersing the nanofibers in ethanol ultrasonic bath and then dropping the suspension onto a Cu grid. The textural characteristics were evaluated by N_2 adsorption measurement on a Belsorp Max apparatus at 77 K (Japan). The specific surface area was determined by Brunauer-Emmett-Teller (BET) method. The pore size distribution (PSD) was calculated according to Non-linear Density Function Theory (NLDFT) method. X-ray photoelectron spectroscopy (XPS, PHI-5,300, USA) was used to characterize the contents and configurations of the nitrogen in the materials.

2.3. Electrochemical measurements

The electrochemical performance was evaluated by galvanostatic cycling and cyclic voltammetry at room temperature in a half-cell, in which lithium foil was used as the counter electrode and 1M $LiPF_6$ was dissolved in a mixture of ethyl carbonate (EC) and dimethyl carbonate (DMC) (1:1, v/v) as the electrolyte. The samples were used as working electrode directly without adding any non-active materials such as polymer binders or electronic conductors. Celgard 2400 was used as separator. The test cells were galvanostatically cycled between 0.01 V-3.0 V vs. Li^+/Li to evaluate the electrochemical performance. Cyclic voltammetry was measured between 0.01-3.0 V vs. Li^+/Li at a scan rate of 0.1 mV s^{-1} by an electrochemical workstation Im6ex (ZAHNER, Germany). The impedance spectra were obtained by applying an AC voltage of 5.0 mV over the frequency range from 0.01 Hz- 2 MHz at room temperature with an electrochemical workstation Im6ex (ZAHNER, Germany) , and software of ZView was employed to fit the collected electrochemical impedance spectroscopy (EIS) data.

3. Results and discussion

3.1. Materials characterization

The macrostructure and microstructure of as-prepared samples is shown in Fig. 1. It can be seen from Fig. 1(a), the morphology of CNFs is randomly oriented and interconnected, which form a porous, non-woven network with diameters varying from tens to hundreds of nanometer and length up to several hundreds of microns. Fig. 1(b) shows the macrostructure of NCNFs. It is clearly seen that the NCNFs have free-standing structure. Actually it has good mechanical integrity which can be freestyle folded and easily cut with conventional cutters or shears, shaped into any required form. As for microstructure of NCNFs (inset of Fig. 1(b)), it is found that NCNFs have non-woven nanofibrous structure and some of beads were observed. Figs. 1(c-d) show the typical morphologies of N-enriched carbon nanofibers, that is, NCNFs and NPCNFs. It can be seen that they have similar morphology of interconnected non-woven nanofibrous structure, which means the non-woven nanofibrous structure can be also well-

maintained after NH_3 treatment. Moreover, it can be clearly observed that carbon nanofibers made from pure PAN precursors have relatively smooth and regular surface morphology. However, after melamine was added, the surface morphology of final carbon nanofibers becomes rough and irregular with obvious beads along the fiber axes. Fig. 1(e) and Fig. 1(f) show the typical TEM images of as-prepared NCNFs and NPCNFs. It is seen that the N-doped carbon nanofibers of sole carbonization show a relatively taut and regular surface structure. However, the nanofibers from carbonization-activation treatment exhibit relatively rough surface morphology and some quantity of pores are created on the surface of NPCNFs. Besides, The disperse rings in the corresponding selected area electron diffraction (SAED) pattern (inset in Fig. 1(e) and Fig. 1(f)) also suggest the NCNFs and NPCNFs are characteristic of amorphous structure of electrospun carbon nanofibers.

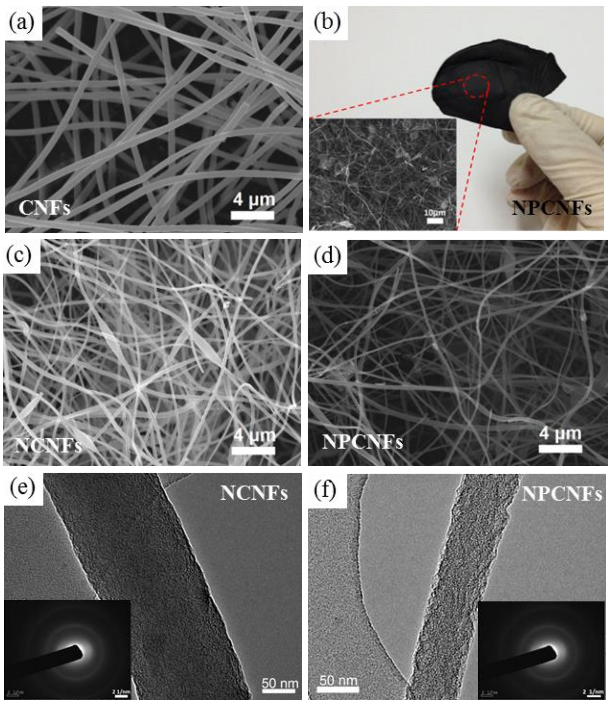

Fig. 1. (a) SEM image of CNFs; (b) Photograph of a free-standing NPCNFs (inset is the microstructure of NPCNFs); SEM images of (c) NCNFs and (d) NPCNFs; TEM images and SAED patterns (insets) of (e) NCNFs and (f) NPCNFs.

N_2 adsorption/desorption measurements are performed at 77 K to characterize the specific surface area and the pore-size distribution (PSD) of different samples, and the isotherms and NLDFT plots are shown in Fig. 2. The isotherms of CNFs, NCNFs and NPCNFs belong to type I pattern according to the IUPAC classification (Fig.2 (a)), indicating three samples are mainly in microporous structures. From the corresponding PSD plotted in Fig. 2(b), it can be seen that micropores dominate in these three kinds of nanofibers obviously. For the sample of NPCNFs-H_2O, a small hysteresis loop can be found in the isotherms plot which indicates the presence of some mesopores. The BET specific surface area and pore volume of all samples is summarized and listed in table 1. Notably, compared with NCNFs and CNFs, the porous carbon nanofibers activated by both NH_3 and H_2O demonstrate much higher BET specific surface area and larger pore volume.

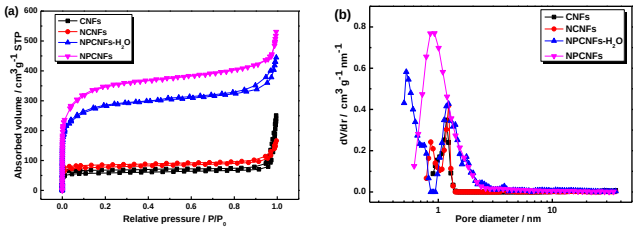

Fig. 2. (a) Nitrogen adsorption–desorption isotherms and (b) pore size distribution of carbonized and activated carbon nanofibers

X-ray photoelectron spectroscopy (XPS) was used to characterize the N doping level and configurations in different samples. As shown in Fig. 3(a), the XPS survey scan spectra show signals of C, O, and N elements for all of the four samples. As expected, the content of nitrogen is increased by adding melamine. However, it is remarkably decreased by H_2O steam activation, but can be increased by NH_3 treatment. The N/C atomic ratios of different samples are summarized in Table 1 based on XPS analysis. The N/C atomic ratio of NPCNFs with NH_3 activation is the highest (7.9%), while NPCNFs-H_2O shows a minimum value of 2.9%. Fig. 3(b-d) shows the binding energy of N_{1s} of the samples. As for CNFs in Fig. 3(b), the complex N_{1s} spectra can be further deconvoluted into three different component peaks at ~398.4 eV, 399.9 eV and 400.9 eV, which can be assigned to the pyridinic (N-6), pyrrolic/pyridone (N-5) and quaternary (N-Q) nitrogen respectively. Remarkably, as shown in the Fig. 3(c) and Fig. 3(d), the N1s XPS fine scan spectra reveal a pair of peaks for NPCNFs-H_2O and NPCNFs, which can be fitted to N-6 nitrogen and N-5 nitrogen for NPCNFs-H_2O, and two well-defined peaks N-Q nitrogen and N-6 nitrogen for NPCNFs, which is believed to be responsible for NH_3 treatment of carbon materials at high temperature [51, 52]. Among these three forms of nitrogen (Fig. 3(e)), according to the reported literatures [14, 15, 42], N-Q nitrogen and N-6 nitrogen are both sp^2 hybridized, can improve the electronic conductivity of carbon host, which thus favorable for enhance electrochemical performance of carbon materials. In addition, especially, N-6 nitrogen is produced predominately via substituting a carbon atom by nitrogen on edges or defect sites of the graphitic carbon layer. This kind of nitrogen is much more chemically active with the low energy barrier for lithium penetrating[41]. And furthermore, N-6 nitrogen can induce a large number of defects, adds Li insertion sites, hence improves the lithium storage capacity and enhances its rate capability for the carbon materials. The content of N-6 nitrogen of all samples is summarized in Table 1. It can be clearly seen that the NPCNFs have highest content of N-6 nitrogen with 38.38%. This value is also higher than those shown in some previous works[15, 35, 46], which indicating, compared with the post modifications, our route provides a facile way for producing a relatively high content of nitrogen, especially of N-6 nitrogen in carbon materials.

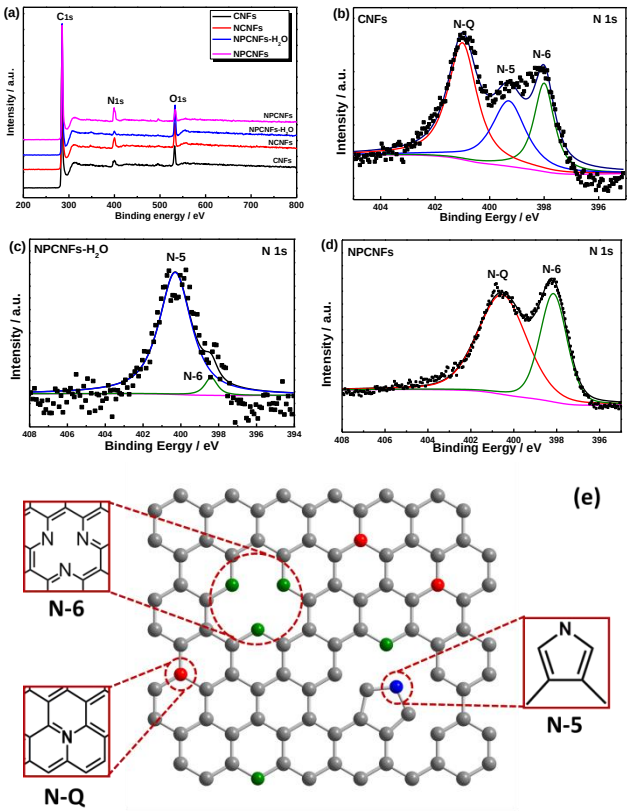

Fig. 3. (a) XPS survey scan spectra of all samples. N 1s fine scan spectra of (b) CNFs, (c) NPCNFs-H_2O and (d) NPCNFs. (e) Schematic illustration of the forms of nitrogen in N-doped carbon materials. The gray spheres represent carbon atoms, red spheres represent quaternary N atoms (N-Q), green spheres represent pyridinic N atoms (N-6), and blue spheres represent pyrrolic N atoms (N-5).

3.2. Electrochemical evaluations

The electrochemical performances of as-obtained porous carbon nanofibers were evaluated using cyclic voltammetry (CV) and deep galvanostatic charge/discharge cycles from 0.01-3.0 V. The collected free-standing nonwoven porous carbon nanofiber networks were directly used as anodes in LIBs, without adding any other polymeric binders or conductive additives. It could remarkably facilitate the high-speed electron transport and hold great potential to enhance the electrochemical performance. As shown in Fig.4 (a), the NPCNFs electrode shows typical CV curves of the porous carbon materials[16, 53]. The distinct peak around 0.1 V in the reduction process demonstrates lithium ions insertion process. And its area is reduced after the first cycle. Fig.4 (b) shows the typical galvanostatic charge/discharge curves of NPCNFs anodes for the initial three cycles and 50th cycle at a current density of 50 mA g^{-1}. The voltage has a sharp drop to a relatively potential plateau at 0.65-0.85 V in the first cycle, which is associated with the formation of solid electrolyte interphase (SEI) film on the electrode due to the decomposition of electrolyte[54]. The initial discharge capacity of NPCNFs is as high as 2245 mAh g^{-1} and the reversible charge capacity is 1323 mAh g^{-1}. The columbic efficiency is 58.9%.The large irreversible capacity can be mainly ascribed to the formation of SEI layer at the surface of NPCNFs and/or the irreversible lithium insertion into special positions in the vicinity of residual H atoms in the carbon material[16, 20, 53]. Nevertheless, the columbic efficiency in the second cycle and thereafter increases over 95% and a stable capacity is achieved. The cycling performance of obtained porous carbon nanofibers at 50 mA g^{-1} is present in Fig.4 (c). It is obvious that the nitrogen-doped porous carbon nanofiber anodes show much improved lithium-ion storage ability compared with non-porous and non-nitrogen doped counterparts. NPCNFs have the largest capacity and a good cycling stability superior to the NPCNFs-H_2O, NCNFs and CNFs, with reversible capacity of 1323 mAh g^{-1} in the first cycle and 1150 mAh g^{-1} in the 50th cycle. The value of first reversible capacity of NPCNFs is higher than most of reported carbon-based anode materials (summarized in table 2), and more than 3 times the theoretical one of commercial graphite (372 mAh g^{-1}). In addition, the 1st reversible capacity of NPCNFs-H_2O is also good as 1233 mAh g^{-1} in the first cycle, but it's cycling stability is not so well. The reversible capacity of NPCNFs-H_2O increases slightly in initial a few cycles but drop sharply to 513 mAh g^{-1} in the 50th cycle. The rate capability of as-prepared porous carbon nanofibers was further investigated. As depicted in Fig.4 (d), the rate performance of NPCNFs is superior to the NPCNFs-H_2O and much better than NCNFs. The NPCNFs anode delivers 1315 mAh g^{-1} at 50 mA g^{-1}, 1145 mAh g^{-1} at 100 mA g^{-1}, 906 mAh g^{-1} at 200 mA g^{-1}, 654 mAh g^{-1} at 500 mA g^{-1}, 473 mAh g^{-1} at 1000 mA g^{-1}. Then the capacity can be recovered to 1163 mAh g^{-1} when the current density is turned back to 50 mA g^{-1}, indicating a good cycling stability and a rate capability.

Table 1 BET specific surface area (m^2 g^{-1}), pore volume (cm^3 g^{-1}), N/C Atomic ratio (%), relative integrated intensities (%) of the X-ray photoelectron spectra of pyridinic nitrogen and EIS fitting results of all samples.

material	SSA[a](m^2 g^{-1})	Total pore volume (cm^3 g^{-1})	N/C Atomic (%)	Pyridinic nitrogen (%)	R_e (Ω)	R_f (Ω)	R_{ct} (Ω)
CNFs	231	0.12	4.1	31.61	8.9	2.5	23.6
NCNFs	305	0.16	7.2	36.24	6.6	3.8	21.3
NPCNFs-H_2O	1056	0.55	2.9	5.47	3.9	1.3	5.9
NPCNFs	1198	0.67	7.9	38.38	2.9	1.6	0.05

a Specific surface area (SSA) was calculated by the Brunauer–Emmett–Teller (BET) method.

To elucidate the resistance change of the obtained porous carbon nanofibers, EIS measurements were performed (Fig. 4 (e)). The impedance of the first Li intercalation of the electrodes was fitted by using the modified Randles equivalent circuit depicted in the inset of Fig. 4 (e). The resistance of electrolyte is denoted as R_e. Here, C_f and R_f denote the capacitance and resistance of the surface film formed on the electrodes, respectively. C_{dl} and R_{ct} correspond to the double-layer capacitance and charge-transfer resistance. The Warburg impedance Z_w is related to the diffusion of lithium ions into the

bulk of a carbon electrode. The numerical value of the diameter of the semicircle in the mid-high frequency on the Z` axis is approximately equal to the charge transfer resistance[14]. The kinetic parameters of all samples are summarized in Table 1. As can be seen from Fig. 4 (e) and Table 1, there is an obvious decrease in the charge transfer resistance after N-doping, indicating that the electronic conductivity of the obtained porous carbon nanofibers was improved by N-doping. However, N-doping is not the singular reason for conductivity increase, as shown by the "anomalous" NPCNFs-H_2O sample. The inclined lines in the low frequency can be attributed to the Warburg impedance, which is associated with lithium ion diffusion in the electrode materials. The lithium ion diffusion coefficient of the electrode is proportional to the slope values[55]. The diffusion coefficient of the NPCNFs also shows the highest mobility for lithium ions diffusion than other samples[56]. The low charge transfer resistance and the high lithium ion diffusion coefficient indicate the good electronic conductivity and high Li-ion transfer speed across interfaces between the electrolyte and active electrode materials, which therefore can enhance the discharge–charge performance and rate capability of the batteries[14, 56, 57]. Fig. 4(f) presents the morphology of NPCNFs after 50th charge-discharge cycles. It is clearly observed that a layer of SEI film was formed at the surface of nanofibers and the interconnected non-woven nanofibrous structure could be well-maintained after deep charge-discharge cycles.

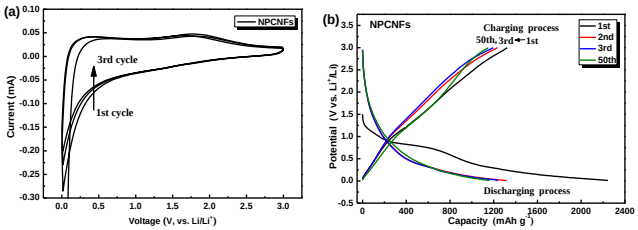

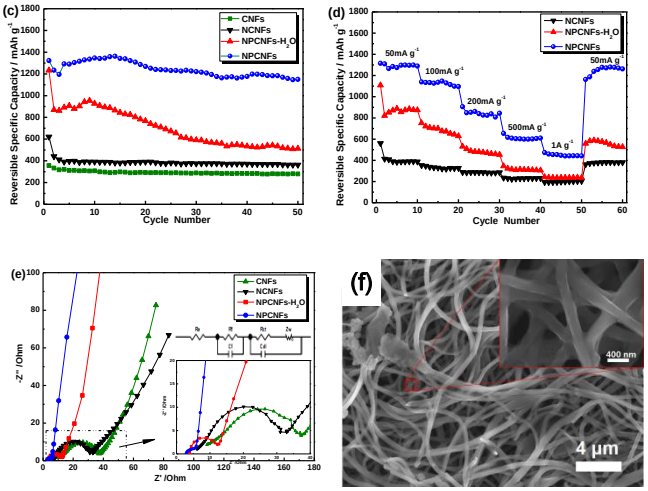

Fig. 4. (a) Cyclic voltammograms and (b) charge/discharge curves of NPCNFs; (c) Cycling performance and (d) rate performance of different samples; (e) Nyquist plots of the EIS recorded for different samples, the upper and lower insets are the corresponding equivalent circuit and the magnification of semicircles, respectively; (f) SEM image of NPCNFs after 50th cycles (inset is the magnified image of NPCNFs after 50th cycles).

Table 2 The electrochemical performances of some carbonaceous anode materials with various microstructures used in Li-ion batteries.

materials	1st cycle reversible capacity (mAh g^{-1})	1st CE[a] (%)	50th cycle reversible capacity (mAh g^{-1})	Test conditions Voltage (V)	Scan rate	Ref.
Commercial PAN fibers	300	--	180 (15th cycle)	0-1.2	25 mA g^{-1}	58
Commercial griaphite	353	80	--	0.005-1.500	C/24	59
SWCNTs	*ca.* 600	30	--	0-3	50 mA g^{-1}	60
MWCNTs	390	33	--	0.02-3.00	30 mA g^{-1}	61
graphene	540	--	290 (20th cycle)	0.01-3.50	50 mA g^{-1}	62
Nitrogen-Doped graphene	832	45	751 (108th cycle)	0.05-3.00	100 mA g^{-1}	63
porous carbon	453	55	459 (100th cycle)	0.005-2.000	50 mA g^{-1}	64
nitrogen-rich mesoporous carbon materials	1029	54	*ca.* 1200 (100th cycle)	0-3	0.1 mA cm^{-2}	15
Carbon hollow nanospheres	772	44	630	0.02-3.00	C/10	7
carbon nanofibers	450	45	--	0-2.8	100 mA g^{-1}	8
porous carbon nanofibers	730	48	445	0-2.5	50 mA g^{-1}	20
Nitrogen-Doped Porous Carbon Nanofiber Webs derived from ppy	1280	48	*ca.* 1300(10 th cycle)	0.01-3.00	100 mA g^{-1}	16
Nitrogen-enriched porous carbon nanofiber networks via electrospinning	1323	59	1150	0.01 -3.00	50 mA g^{-1}	This work

a The 1st cycle columbic efficiency.

The ultrahigh capacity and good rate capability of NPCNFs can be ascribed to its unique free-standing porous nanofibrous structure and relatively high-level of nitrogen doping. Firstly, the large surface area of NPCNFs offers sufficient electrode/electrolyte interface to absorb Li-ion and the resided micropores provide facile channels for Li-ion diffusion and may act as reservoirs for storage of Li-ion[65]. Secondly, higher N doping levels in carbon materials lead to higher charge

(reversible) capacities because nitrogen doping can enhance the electrochemical reactivity and electronic conductivity. In addition, especially, the large amount of pyridinic nitrogen in as-obtained NPCNFs can induce a large number of defects, more Li^+ insertion sites and thus enhances the lithium storage capacity of the carbon materials. In addition, the large adsorption energies of the Li ions at the pyridine-like defect and the low energy barrier for lithium penetrating the defect ensure its capability for lithium storage. Thirdly, the interconnected conducting nanofibrous network and elimination of insulating binders ensure fast electron transfer for rapid Faradiac reaction and the nanosized fibers can shorten the ionic transport length. Last but not the least, the large void space in the free-standing NPCNFs anode can effectively alleviate the volume change during the lithiation/delithiation process, while the strong mechanical integrity of NPCNFs can prevent the electrode from pulverization.

Conclusions

In summary, we have successfully prepared the nitrogen-enriched porous carbon nanofiber networks, by using low-cost melamine and polyacrylonitrile as precursors, through electrospinning along with the subsequent carbonization and NH_3 treatment. As free-standing anodes for LIBs, the large surface area, well-developed microporous structure, high nitrogen doping level and great amount of pyridinic nitrogen make the NPCNFs show an ultrahigh capacity of 1323 mAh g^{-1} in the first cycle, good cycling stability and rate capability. These interesting features could make the NPCNFs a potentially useful anode material for high-performance LIBs if their initial capacity loss problem can be satisfactorily addressed.

Acknowledgements

The authors thank the funds from the 973 program of China (No.2014CB932401) and the National Natural Science Foundation of China (No. 51232005). This work is also supported by Ministry of Science and Technology (MOST) of China under Grant 2010DFA72760, Collaboration on cutting-edge technology development of electric vehicle.

Notes and references

[a] State Key Laboratory of New Ceramics and Fine Processing, School of Materials Science and Engineering, Tsinghua University, Beijing 100084, China

[b] Key Laboratory of Advanced Materials (MOE), School of Materials Science and Engineering, Tsinghua University, Beijing 100084, China

[c] City Key Laboratory of Thermal Management Engineering and Materials, Graduate School at Shenzhen, Tsinghua University, Shenzhen, Guangdong 518055, China

[d] School of Materials Science and Engineering, Inner Mongolia University of Technology, Aimin Street 49, Hohhot 010051, China

* Corresponding author. Tel: +86 10 62773752; Fax: +86 10 62771160.
E-mail address: fykang@mail.tsinghua.edu.cn (F. Kang) and zhhuang@mail.tsinghua.edu.cn (Z. Huang)

1. M. Armand and J.-M. Tarascon, *Nature*, 2008, 451, 652-657.
2. B. Dunn, H. Kamath and J.-M. Tarascon, *Science*, 2011, 334, 928-935.
3. J. Liu, J. G. Zhang, Z. Yang, J. P. Lemmon, C. Imhoff, G. L. Graff, L. Li, J. Hu, C. Wang and J. Xiao, *Advanced Functional Materials*, 2013, 23, 929-946.
4. J.-M. Tarascon and M. Armand, *Nature*, 2001, 414, 359-367.
5. M. M. Thackeray, C. Wolverton and E. D. Isaacs, *Energy & Environmental Science*, 2012, 5, 7854-7863.
6. B. Guo, X. Wang, P. F. Fulvio, M. Chi, S. M. Mahurin, X. G. Sun and S. Dai, *Advanced materials*, 2011, 23, 4661-4666.
7. F.-D. Han, Y.-J. Bai, R. Liu, B. Yao, Y.-X. Qi, N. Lun and J.-X. Zhang, *Advanced Energy Materials*, 2011, 1, 798-801.
8. C. Kim, K. S. Yang, M. Kojima, K. Yoshida, Y. J. Kim, Y. A. Kim and M. Endo, *Advanced Functional Materials*, 2006, 16, 2393-2397.
9. B. J. Landi, M. J. Ganter, C. D. Cress, R. A. DiLeo and R. P. Raffaelle, *Energy & Environmental Science*, 2009, 2, 638-654.
10. K. T. Lee, J. C. Lytle, N. S. Ergang, S. M. Oh and A. Stein, *Advanced Functional Materials*, 2005, 15, 547-556.
11. H. Wang, T. Abe, S. Maruyama, Y. Iriyama, Z. Ogumi and K. Yoshikawa, *Advanced materials*, 2005, 17, 2857-2860.
12. Z.-S. Wu, W. Ren, L. Xu, F. Li and H.-M. Cheng, *ACS Nano*, 2011, 5, 5463-5471.
13. H. Zhou, S. Zhu, M. Hibino, I. Honma and M. Ichihara, *Advanced materials*, 2003, 15, 2107-2111.
14. C. Hu, Y. Xiao, Y. Zhao, N. Chen, Z. Zhang, M. Cao and L. Qu, *Nanoscale*, 2013, 5, 2726-2733.
15. Y. Mao, H. Duan, B. Xu, L. Zhang, Y. Hu, C. Zhao, Z. Wang, L. Chen and Y. Yang, *Energy & Environmental Science*, 2012, 5, 7950-7955.
16. L. Qie, W.-M. Chen, Z.-H. Wang, Q.-G. Shao, X. Li, L.-X. Yuan, X.-L. Hu, W.-X. Zhang and Y.-H. Huang, *Advanced Materials*, 2012, 24, 2047-2050.
17. L. Ji, Z. Lin, A. J. Medford and X. Zhang, *Carbon*, 2009, 47, 3346-3354.
18. L. Ji and X. Zhang, *Nanotechnology*, 2009, 20, 155705-155711.
19. C. Li, X. Yin, L. Chen, Q. Li and T. Wang, *Journal of Physical Chemistry C*, 2009, 113, 13438-13442.
20. D. Nan, J.-G. Wang, Z.-H. Huang, L. Wang, W. Shen and F. Kang, *Electrochemistry Communications*, 2013, 34, 52–55.
21. L. Qie, W.-M. Chen, Z.-H. Wang, Q.-G. Shao, X. Li, L.-X. Yuan, X.-L. Hu, W.-X. Zhang and Y.-H. Huang, *Advanced materials* 2012, 24, 2047-2050.
22. X.-L. Wu, L.-L. Chen, S. Xin, Y.-X. Yin, Y.-G. Guo, Q.-S. Kong and Y.-Z. Xia, *Chemsuschem*, 2010, 3, 703-707.
23. T. Nokami, T. Matsuo, Y. Inatomi, N. Hojo, T. Tsukagoshi, H. Yoshizawa, A. Shimizu, H. Kuramoto, K. Komae, H. Tsuyama and J.-i. Yoshida, *Journal of the American Chemical Society*, 2012, 134, 19694-19700.
24. C.-M. Park, J.-H. Kim, H. Kim and H.-J. Sohn, *Chemical Society Reviews*, 2010, 39, 3115-3141.
25. M. V. Reddy, G. V. Subba Rao and B. V. R. Chowdari, *Chemical reviews*, 2013, 113, 5364-5457.
26. Y. Idota, T. Kubota, A. Matsufuji, Y. Maekawa and T. Miyasaka, *Science*, 1997, 276, 1395-1397.
27. J. Zhang, Y.-S. Hu, J.-P. Tessonnier, G. Weinberg, J. Maier, R. Schlögl and D. S. Su, *Advanced materials*, 2008, 20, 1450-1455.
28. Z. Li, G. Wu, D. Liu, W. Wu, B. Jiang, J. Zheng, Y. Li, J. Li and M. Wu, *J. Mater. Chem. A*, 2014, 2, 7471-7477.
29. T. Tran, J. Feikert, X. Song and K. Kinoshita, *Journal of The Electrochemical Society*, 1995, 142, 3297-3302.
30. Y. Wu, S. Fang and Y. Jiang, *J. Mater. Chem.*, 1998, 8, 2223-2227.
31. Y. Wu, S. Fang, Y. Jiang and R. Holze, *Journal of Power Sources*, 2002, 108, 245-249.
32. M. Endo, C. Kim, T. Karaki, Y. Nishimura, M. Matthews, S. Brown and M. Dresselhaus, *Carbon*, 1999, 37, 561-568.
33. C. Kim, T. Fujino, T. Hayashi, M. Endo and M. Dresselhaus, *Journal of The Electrochemical Society*, 2000, 147, 1265-1270.
34. B. Way and J. Dahn, *Journal of The Electrochemical Society*, 1994, 141, 907-912.
35. L. G. Bulusheva, A. V. Okotrub, A. G. Kurenya, H. Zhang, H. Zhang, X. Chen and H. Song, *Carbon*, 2011, 49, 4013-4023.
36. P. Han, Y. Yue, L. Zhang, H. Xu, Z. Liu, K. Zhang, C. Zhang, S. Dong, W. Ma and G. Cui, *Carbon*, 2012, 50, 1355-1362.
37. X. Huang, R. Zhang, X. Zhang, G. Wen, H. Yu and Y. Zhou, *Scripta Materialia*, 2012, 67, 987-990.
38. H. Li, L. Shen, X. Zhang, J. Wang, P. Nie, Q. Che and B. Ding, *Journal of Power Sources*, 2013, 221, 122-127.
39. X. Li, D. Geng, Y. Zhang, X. Meng, R. Li and X. Sun, *Electrochemistry Communications*, 2011, 13, 822-825.

40. X. Li, J. Liu, Y. Zhang, Y. Li, H. Liu, X. Meng, J. Yang, D. Geng, D. Wang, R. Li and X. Sun, *Journal of Power Sources*, 2012, 197, 238-245.
41. C. Ma, X. Shao and D. Cao, *Journal of Materials Chemistry*, 2012, 22, 8911-8915.
42. A. L. M. Reddy, A. Srivastava, S. R. Gowda, H. Gullapalli, M. Dubey and P. M. Ajayan, *Acs Nano*, 2010, 4, 6337-6342.
43. W. H. Shin, H. M. Jeong, B. G. Kim, J. K. Kang and J. W. Choi, *Nano Letters*, 2012, 12, 2283-2288.
44. H. Wang, C. Zhang, Z. Liu, L. Wang, P. Han, H. Xu, K. Zhang, S. Dong, J. Yao and G. Cui, *Journal of Materials Chemistry*, 2011, 21, 5430-5434.
45. L. Xifei, L. Jian, Z. Yong, L. Yongliang, L. Hao, M. Xiangbo, Y. Jinli, G. Dongsheng, W. Dongniu, L. Ruying and S. Xueliang, *Journal of Power Sources*, 2012, 197, 238-245.
46. S. Yang, L. Zhi, K. Tang, X. Feng, J. Maier and K. Muellen, *Advanced Functional Materials*, 2012, 22, 3634-3640.
47. K. Zhang, P. Han, L. Gu, L. Zhang, Z. Liu, Q. Kong, C. Zhang, S. Dong, Z. Zhang, J. Yao, H. Xu, G. Cui and L. Chen, *Acs Applied Materials & Interfaces*, 2012, 4, 658-664.
48. M. Morita, T. Hanada, H. Tsutsumi, Y. Matsuda and M. Kawaguchi, *Journal of The Electrochemical Society*, 1992, 139, 1227-1230.
49. B. Zhang, Y. Yu, Z. L. Xu, S. Abouali, M. Akbari, Y. B. He, F. Y. Kang and J. K. Kim, *Advanced Energy Materials*, 2014, 4, 1301448-1301457.
50. K. Chan, J. Young Il, N. Bui Thi Nhu, Y. Kap Seung, M. Kojima, Y. A. Kim, M. Endo and J. W. Lee, *Small*, 2007, 3, 91-95.
51. X. Li, H. Wang, J. T. Robinson, H. Sanchez, G. Diankov and H. Dai, *Journal of the American Chemical Society*, 2009, 131, 15939-15944.
52. C. L. Mangun, K. R. Benak, J. Economy and K. L. Foster, *Carbon*, 2001, 39, 1809-1820.
53. F. D. Han, Y. J. Bai, R. Liu, B. Yao, Y. X. Qi, N. Lun and J. X. Zhang, *Advanced Energy Materials*, 2011, 1, 798-801.
54. C. Kim, K. S. Yang, M. Kojima, K. Yoshida, Y. J. Kim, Y. A. Kim and M. Endo, *Advanced Functional Materials*, 2006, 16, 2393-2397.
55. Y. S. Hu, P. Adelhelm, B. M. Smarsly, S. Hore, M. Antonietti and J. Maier, *Advanced Functional Materials*, 2007, 17, 1873-1878.
56. X.-L. Wu, Q. Liu, Y.-G. Guo and W.-G. Song, *Electrochemistry Communications*, 2009, 11, 1468-1471.
57. G. Zou, D. Zhang, C. Dong, H. Li, K. Xiong, L. Fei and Y. Qian, *Carbon*, 2006, 44, 828-832.
58. J. K. Lee, K. W. An, J. B. Ju, B. W. Cho, W. I. Cho, D. Park and K. S. Yun, *Carbon*, 2001, 39, 1299-1305.
59. T. D. Tran, J. H. Feikert, X. Song and K. Kinoshita, *Journal of the Electrochemical Society*, 1995, 142, 3297-3302.
60. B. Gao, A. Kleinhammes, X. P. Tang, C. Bower, L. Fleming, Y. Wu and O. Zhou, *Chemical Physics Letters*, 1999, 307, 153-157.
61. F. Leroux, K. Méténier, S. Gautier, E. Frackowiak, S. Bonnamy and F. Béguin, *Journal of Power Sources*, 1999, 81–82, 317-322.
62. E. Yoo, J. Kim, E. Hosono, H. Zhou, T. Kudo and I. Honma, *Nano Letters*, 2008, 8, 2277-2282.
63. L. L. Tian, X. Y. Wei, Q. C. Zhuang, C. H. Jiang, C. Wu, G. Y. Ma, X. Zhao, Z. M. Zong and S. G. Sun, *Nanoscale*, 2014, 6, 6075-6083.
64. L. Zhang, M. J. Zhang, Y. H. Wang, Z. L. Zhang, G. W. Kan, C. G. Wang, Z. Y. Zhong and F. B. Su, *J. Mater. Chem. A*, 2014, 2, 10161-10168.
65. N. A. Kaskhedikar and J. Maier, *Advanced Materials*, 2009, 21, 2664-2680.